

S.1. Synthetic Earthquake Catalog, and Master Rupture Sequence

In this section, we discuss the methodology used to identify the time-period corresponding to the real-world GPS-velocity measurements in our simulated time-series. We first set the end-time for each asperity's synthetic rupture sequence as the time of the most recent observed rupture on that asperity. We use these most recent ruptures as the ‘seeds’ for building synthetic catalogs for the APRE and APOST asperity configurations. We assign ruptures to each asperity at its characteristic rupture interval, ΔT_R (Table 2), starting with the ‘seed’ rupture, and going backward in time for a sufficiently large number of ruptures. The end-time for the observed GPS velocity calculations time, T_{GPS} (the year 2000; right edge of Figure S-1b), occurs after a fixed duration from this most recent rupture in the catalog (6 years since the 1994 M_w 7.8 Sanriku-oki event, the last major rupture in our modeled region prior to 2000). We call the duration between the oldest ‘seed’ rupture incorporated into the catalog, and T_{GPS} , the current rupture sequence (CRS).

Since the fixed rupture intervals assumed for different asperities are not simply related to each other, the sequence of ruptures corresponding to the CRS will only occur at specific times in our catalog. Specifically, the time-interval between successive repetitions of the CRS is arithmetically equal to the least common multiple (LCM) of all the asperity rupture intervals in our model, T_{LCM} . The sequence of ruptures over ANY time-period corresponding to T_{LCM} will be identical, by definition. For the APRE and APOST configurations, $T_{LCM} = 600$ yrs, and 9000 yrs, respectively. T_{LCM} is also the time over which mean fault tractions and creep rates return to that required for steady-state plate subduction, and the mean slip on all patches catches up to that predicted by the plate-convergence rate (i.e., $V_P T_{LCM}$). This time period therefore defines the ‘seismic-cycle’ for a specific model asperity configuration.

We start a simulation at the beginning of this synthetic catalog. We then find the smallest integral multiple of T_{LCM} beyond which model stresses have spun-up (Figures 3 and 4). We locate T_{GPS} at the end of this spun-up seismic cycle. The starting time, T_{start} , for velocity calculations is then determined by the duration over which the observed GPS velocities were computed. For all our simulations, the GPS observation period, $T_{start} - T_{GPS}$, corresponds to the years 1996 – 2000 (Figure S-1, Figure 4-inset, and middle columns of Figure 6a,b).

SUPPLEMENTARY MATERIAL: Kanda et al., 2012

If one of the rupture intervals were off by even one year, T_{LCM} will be significantly longer, by definition of the LCM. Thus, T_{LCM} is very sensitive to the actual rupture intervals chosen, which depend not only on the exact asperity size, but also on the mesh resolution used. However, we find in our simulations that more recent ruptures (over the last 4-5 decades) are significantly more important than earlier ones, for the range of fault frictional parameter values considered here. Therefore, the exact timing of older events does not matter as much for calculating present-day GPS velocities. Hence, to avoid unnecessarily extending simulation time without significantly improving model predictions at T_{GPS} , we round rupture intervals to the nearest 5 years in Table 2.

SUPPLEMENTARY MATERIAL: Kanda et al., 2012

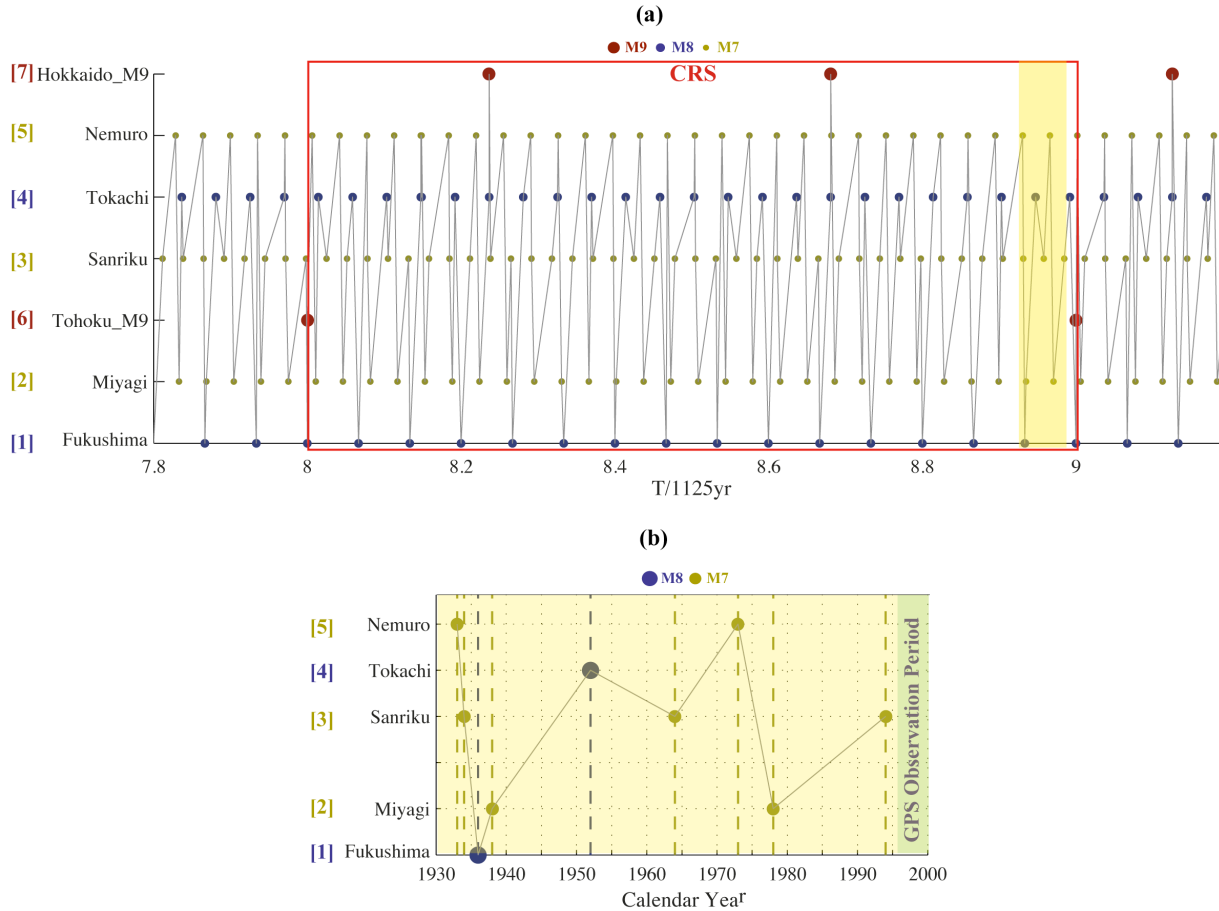


Figure S-1. (a) Synthetic rupture sequence for the APOST configuration. Time (x-axis) is normalized by the fixed rupture interval of the largest asperity ('Tohoku-M9', maroon circles), $\Delta T_{R, Tohoku9} = 1125$ yrs. This complex rupture sequence is generated by assuming that all model asperities rupture at fixed intervals given in Table 2. Asperity numbers are identical to those in Table 2 and Figure 1. Each filled circle represents a rupture, with its size and color indicating characteristic rupture magnitude. The current rupture sequence (CRS, red rectangle), containing the latest ruptures on all of the APOST asperities (observed or inferred), repeats every $8\Delta T_{R, Tohoku9}$, or 9000 years (and corresponds to the last ΔT_R of this time-interval). Yellow shaded patch indicates the time-period shown in (b). (b) Zoom-in of the CRS over a 60 year time interval prior to the GPS observation period (1996-2000, green shading). Only asperities that ruptured during this time interval are shown.

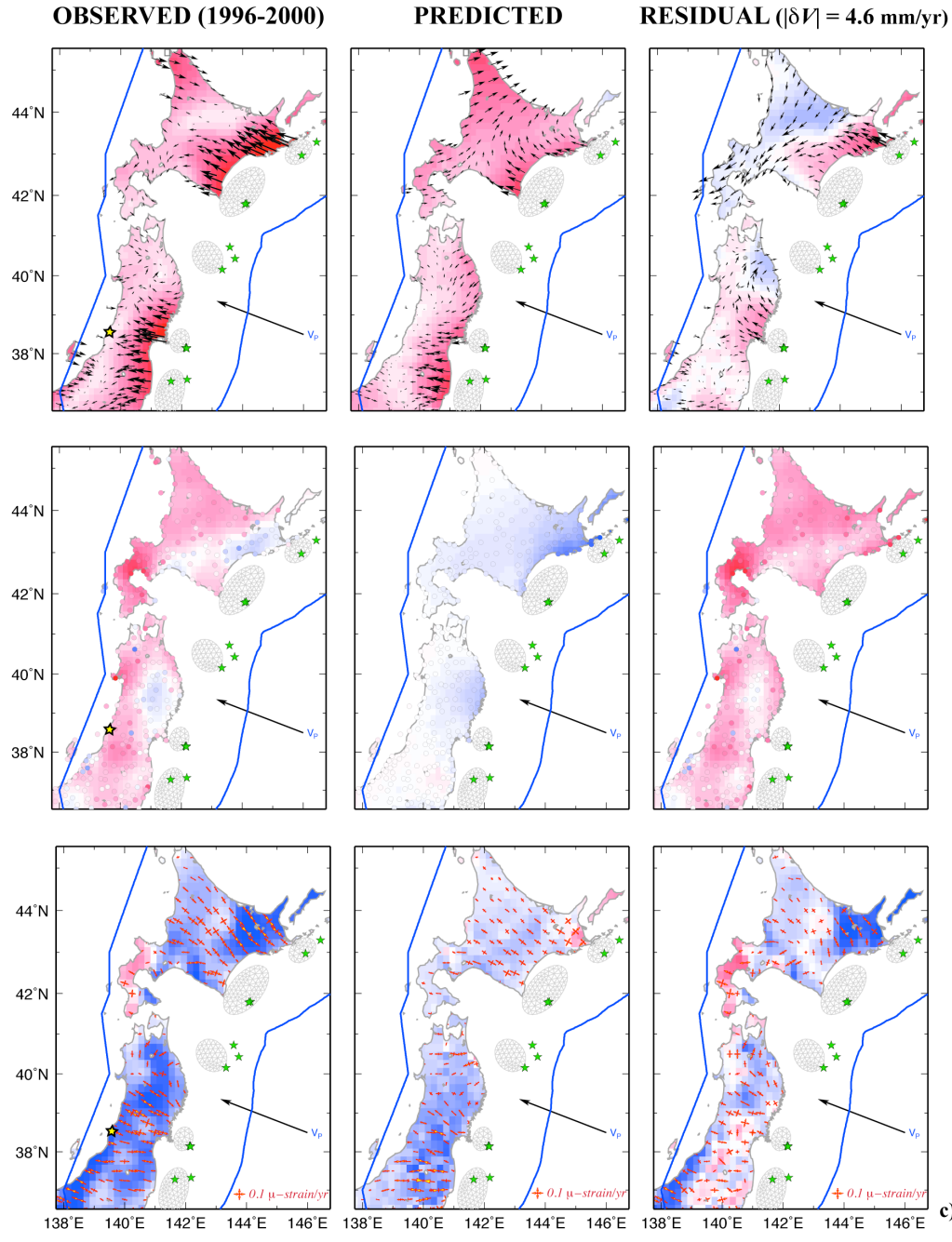


Figure S-2. Observed GPS velocities (left column: top and middle panels) and corresponding dilatation-rates (left column: bottom panel) compared with model predictions (middle column) and residuals (observed – modeled, right column) for the APRE configuration and assuming a frictionless fault, *APRE- α 0*. Magnitude of mean residual velocity, $|\delta V|$, is shown at the top of the right column. Plate convergence velocity vector is shown in each panel for scale. The scale for principal strain crosses is shown in each of the bottom panels. Green stars represent the epicenters of major recorded earthquakes during the past 75 years. Yellow star in the left column represents the reference station (Geonet #940034).

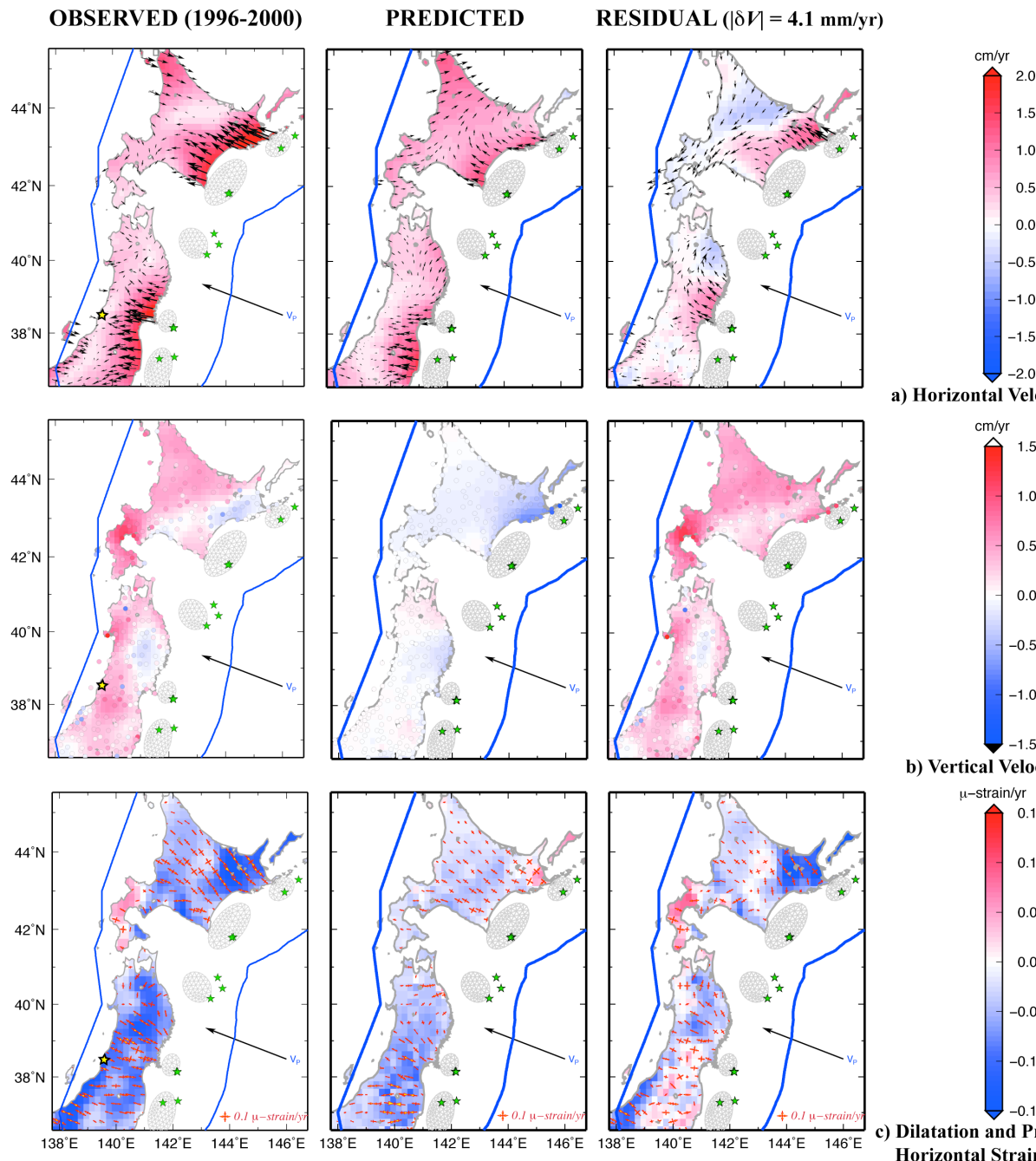


Figure S-3. Observed GPS velocities (left column: top and middle panels) and corresponding dilatation-rates (left column: bottom panel) compared with model predictions (middle column) and residuals (observed – modeled, right column) for the APRE configuration and weak rate-strengthening rheology, $APRE-\alpha 0.01$. All scales and symbols are identical to that for Figure S-2.

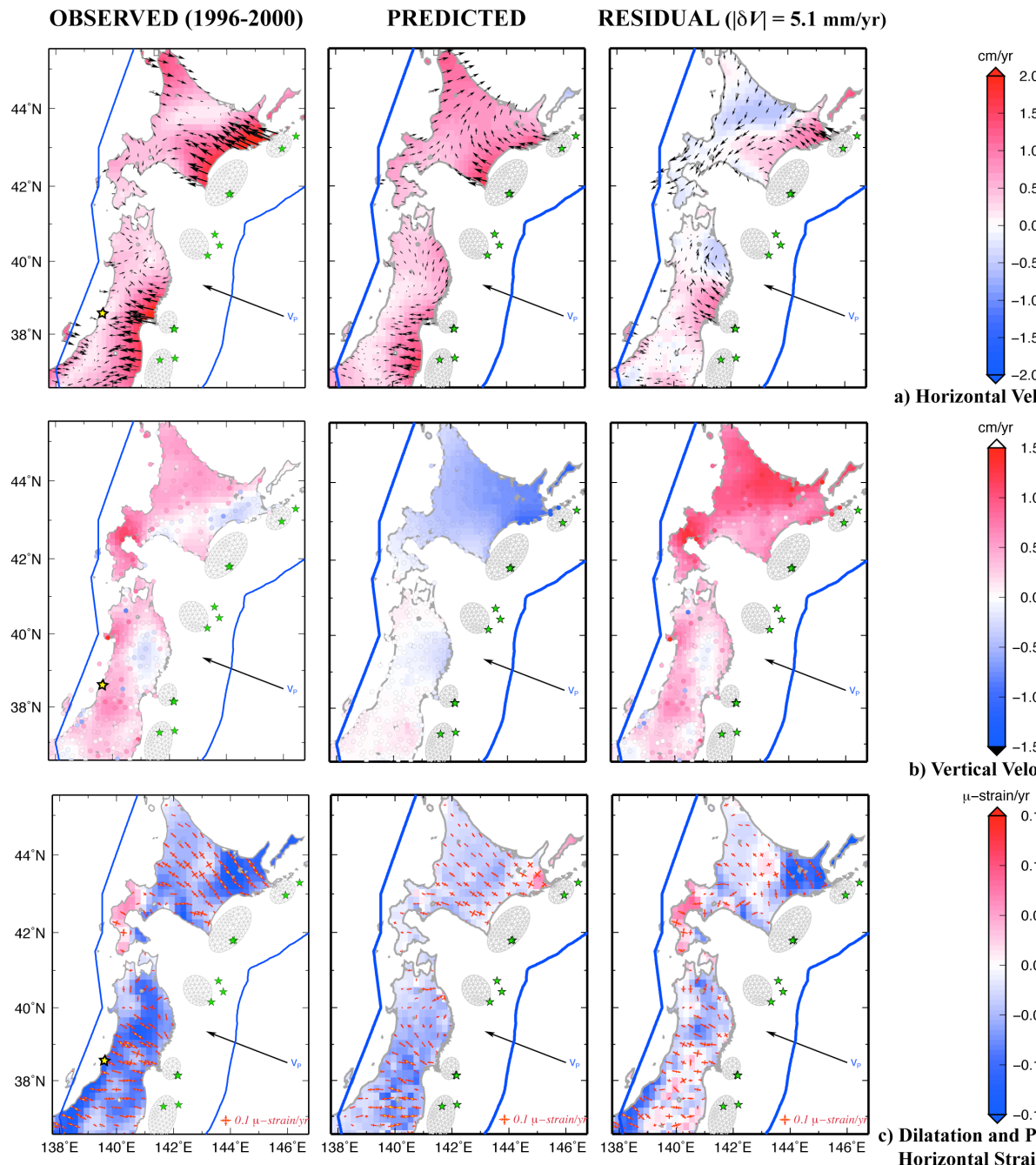


Figure S-4. Observed GPS velocities (left column: top and middle panels) and corresponding dilatation-rates (left column: bottom panel) compared with model predictions (middle column) and residuals (observed – modeled, right column) for the APRE configuration and strong rate-strengthening rheology, APRE- α 0.10. All scales and symbols are identical to that for Figure S-2.

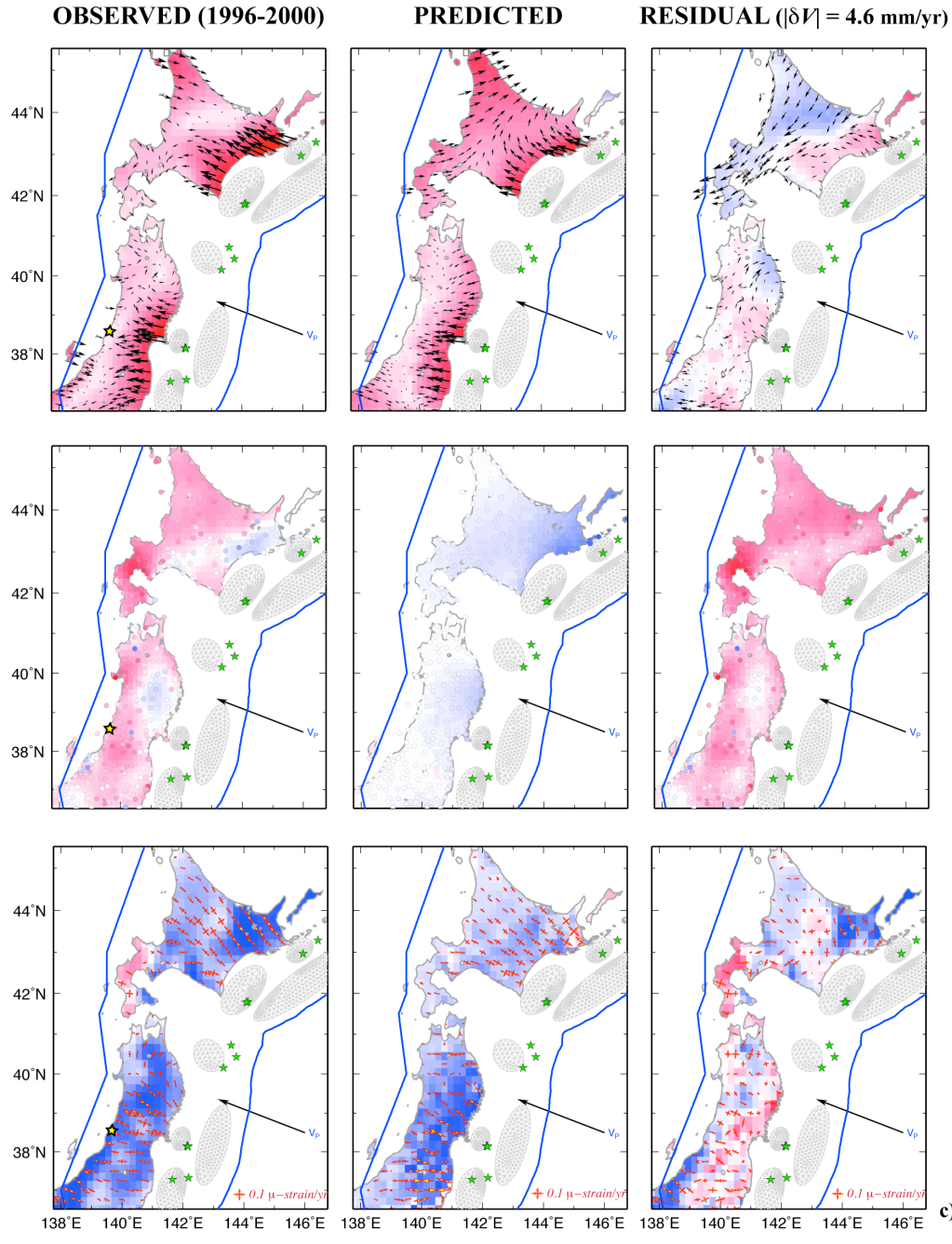


Figure S-5. Observed GPS velocities (left column: top and middle panels) and corresponding dilatation-rates (left column: bottom panel) compared with model predictions (middle column) and residuals (observed – modeled, right column) for APOST configuration and assuming a frictionless fault, *APOST- α 0*. All scales and symbols are identical to that for Figure S-2.

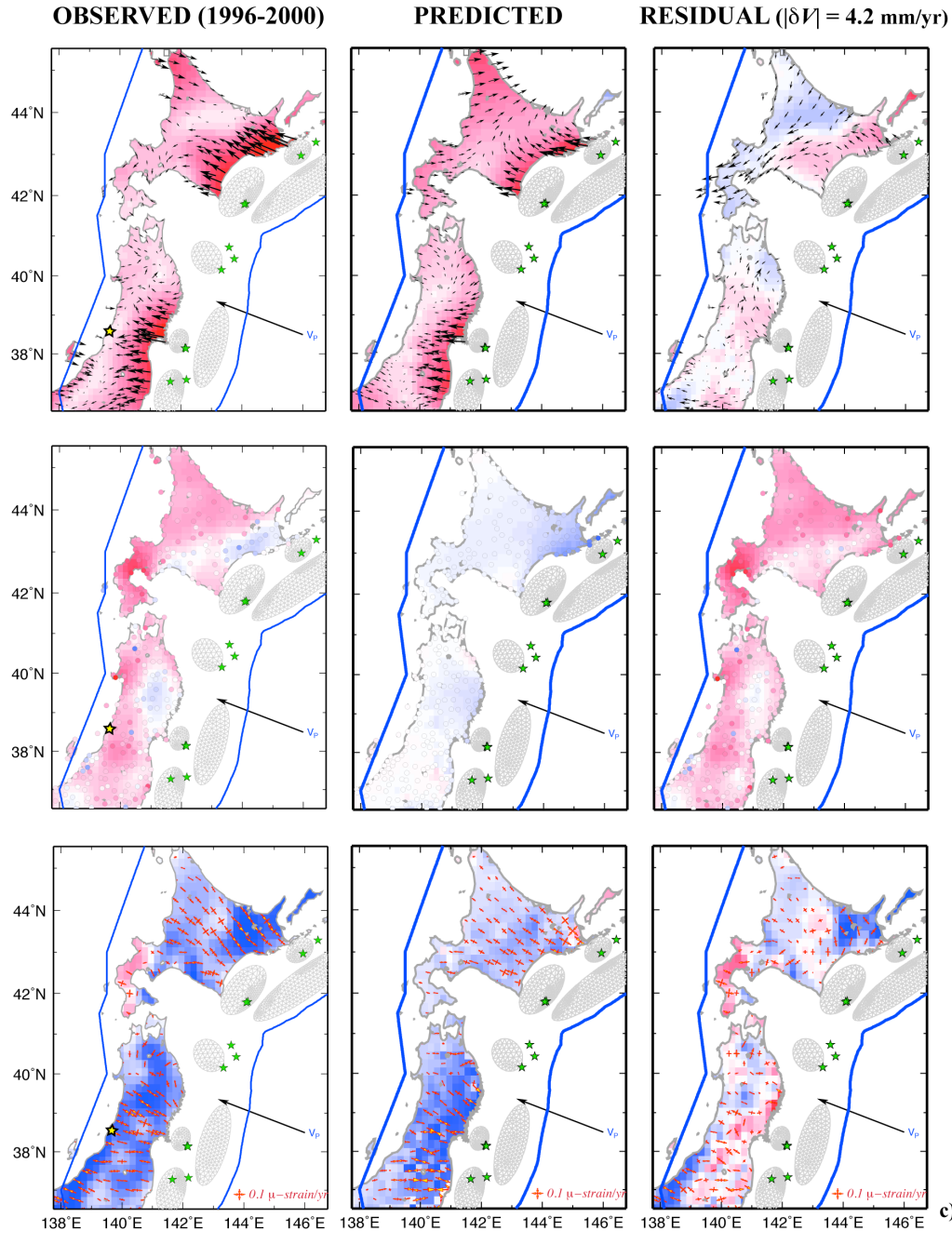


Figure S-6. Observed GPS velocities (left column: top and middle panels) and corresponding dilatation-rates (left column: bottom panel) compared with model predictions (middle column) and residuals (observed – modeled, right column) for the APOST configuration and weak rate-strengthening rheology, *APOST- α 0.01*. All scales and symbols are identical to that for Figure S-2.

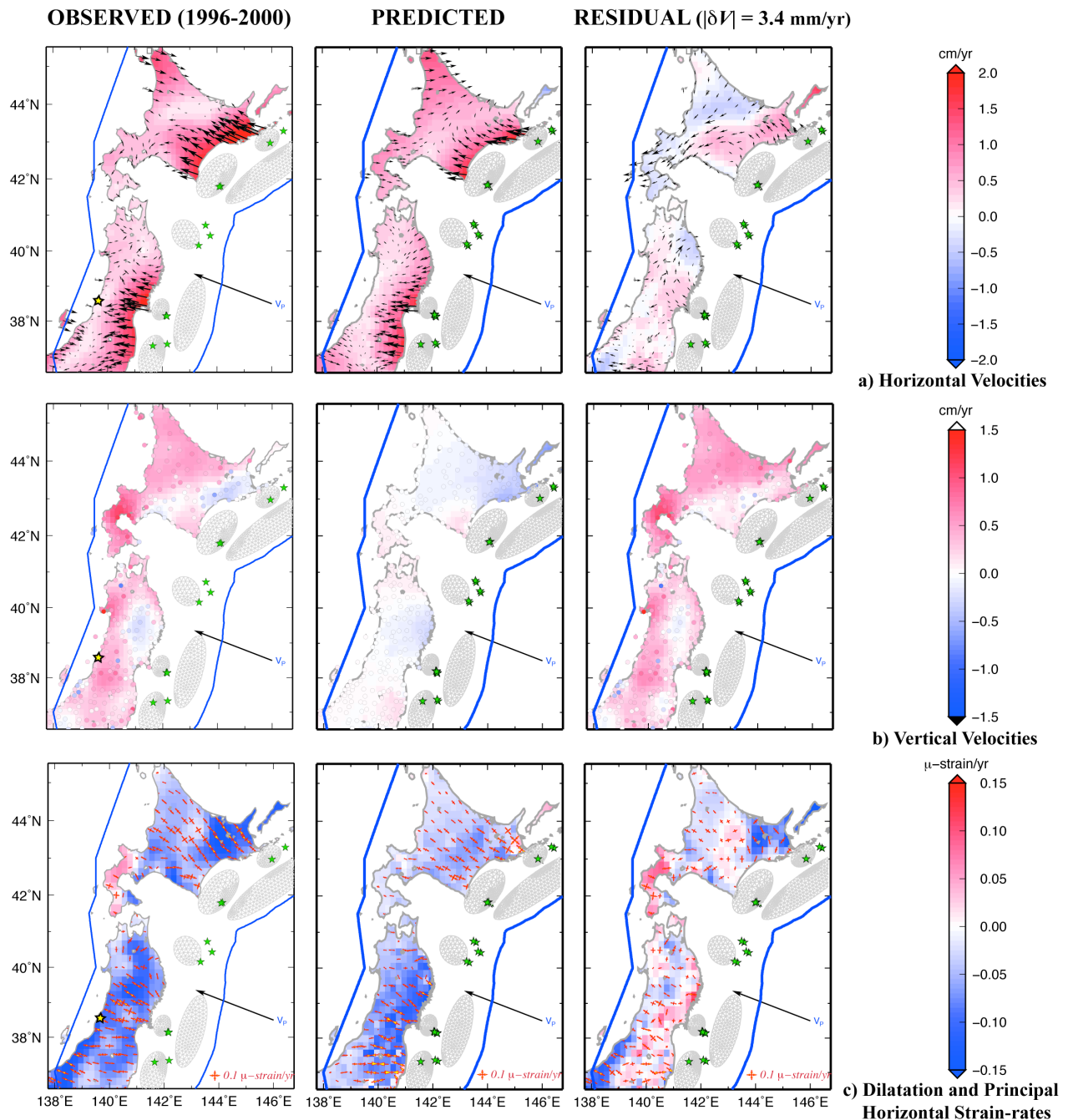


Figure S-7. Observed GPS velocities (left column: top and middle panels) and corresponding dilatation-rates (left column: bottom panel) compared with model predictions (middle column) and residuals (observed – modeled, right column) for the APOST configuration and strong rate-strengthening rheology, *APOST- α 0.10*. All scales and symbols are identical to that for Figure S-2